MULTIGROUP DIFFUSION KINETICS BENCHMARK OF AN ADS SYSTEM IN SLAB GEOMETRY

by

B.D. Ganapol[+], E.H. Mund[*], P. Ravetto[#] and M.M. Rostagno[#]

+ Department of Aerospace and Mechanical Engineering
University of Arizona
Tucson, AZ 85721-0119 (USA)

* Service de Métrologie Nucléaire
Université Libre de Bruxelles
1050 Brussels (Belgium)
emund@ulb.ac.be

Dipartimento di Energetica
Politecnico di Torino
Corso Duca degli Abruzzi, 24
10129 Torino (Italy)

ABSTRACT

The paper is devoted to the construction of a benchmark for the neutron kinetics of a subcritical source-driven system. A two-group diffusion model is adopted in multi-region slab geometry, for a configuration typical of the MYRRHA system proposed by the Mol Nuclear Center (Belgium). The steady-state equations are solved analytically and by Mathematica. The time-dependent solution is obtained by a well-assessed Laplace transform inversion technique. Results are compared to a direct finite-difference numerical solution and also to point kinetics.

1. INTRODUCTION

Accelerator Driven Systems (ADS) combining a neutron spallation source and a subcritical lattice have gained worldwide interest, both as a potential tool for the elimination of long-lived minor actinides in the nuclear waste legacy of Generation II reactors, and (to a lesser extent) as 'energy amplifiers' for power production (See [1-2]). A primary motivation for the nuclear waste transmutation in ADS systems lies in the fact that the important (fissile) minor actinides have a low value of delayed neutron fraction β, and therefore are difficult to eliminate in classical (i.e. critical) reactors, for safety reasons. Indeed, the fission burning of large quantities of minor activities in critical systems would drastically reduce the prompt criticality safety margin to intolerable values. In subcritical systems with an external neutron source this problem is attenuated, since the superprompt criticality margin may be larger. This particular feature however, does not eliminate the need to properly assess the

safety of ADS concepts. Hence, the necessity to develop benchmark solutions to some simple, though meaningful, transients as considered in this paper.

An interesting feature of subcritical systems with external neutron sources lies in the fact that they allow analytical multigroup diffusion benchmark solutions to be built much more easily than critical systems. This is due to the fact that in the former case the problem is linear (with an additional evaluation of the multiplication factor), whereas for critical systems the problem is essentially nonlinear, involving the product of the unknown multiplication factor and neutron fluxes. In this paper, we present such an analytical solution for a two-group time-dependent problem in plane geometry. For the purpose of illustration, we analyze some transients in a 1D model of the ADS MYRRHA concept developed at the Mol Nuclear Center (see for instance [1]). MYRRHA is a small liquid metal cooled fast subcritical core with an hexagonal lattice. Spallation neutrons extend the energy spectrum largely above 10 MeV. In such a system, transport effects are meaningful and the present study is therefore clearly an approximation of physical reality. But since an analytical solution can be obtained and the solution technique is readily extendable to larger number of groups, it deserves some careful attention. Section 2 of the paper gives some details about the physical model. Sections 3 and 4 describe the steady state and transient benchmark solutions, respectively. Section 5 gives numerical results and Section 6 draws the conclusion.

2. THE PHYSICAL/MATHEMATICAL ADS MODEL

We adopt the one-dimensional geometry shown in Fig.1 comprising four regions: a spallation source, two fission layers and a reflector. The reactor is symmetrical about the centerline ($x = 0$), with homogeneous regions. The first layer at left is the Pb-Bi spallation source. It is surrounded by two layers of fissile material with different fuel contents (30% MOX in the inner layer and a mixture of 20% and 30% MOX in the outer layer). A Pb-Bi reflector acts as a radiation shield to protect the environment. Zero flux boundary conditions are imposed at the outer reflector surface (extrapolated endpoint is assumed in the reactor dimension) and a symmetry condition applies at the reactor center.
The ADS transient behavior analyzed here will be characterized by a two-group reactor kinetic mathematical model as described by

$$\frac{1}{\mathrm{v}_1}\frac{\partial \phi_1(x,t)}{\partial t} = \frac{\partial}{\partial x}\left[D_1(x)\frac{\partial \phi_1(x,t)}{\partial x}\right] - \Sigma_{r1}(x)\phi_1(x,t) + (1-\beta)\nu\Sigma_{f1}(x)\phi_1(x,t) + \\ + (1-\beta)\nu\Sigma_{f2}(x)\phi_2(x,t) + \lambda C(x,t) + Q_1(x,t),$$

$$\frac{1}{\mathrm{v}_2}\frac{\partial \phi_2(x,t)}{\partial t} = \frac{\partial}{\partial x}\left[D_2(x)\frac{\partial \phi_2(x,t)}{\partial x}\right] - \Sigma_{r2}(x)\phi_2(x,t) + \Sigma_{12}(x)\phi_1(x,t) + Q_2(x,t),$$

and

$$\frac{\partial C(x,t)}{\partial t} + \lambda C(x,t) = \beta\left[\nu\Sigma_{f1}(x)\phi_1(x,t) + \nu\Sigma_{f2}(x)\phi_2(x,t)\right] \ .$$

Adjacent group down scatter from group 1 to group 2 is allowed and only one delayed neutron precursor is assumed. In addition, the following assumptions are made:

a) fission neutrons appear only in group 1 while fission occurs in both neutron groups,
b) the spallation source has a component in the both groups and is uniformly distributed in the first region
c) the ADS is made of four slab layers each with homogeneous neutron properties as given in Table 1 and kinetic parameters as given in Table 2
d) initial conditions and source traces will be specified for several specific transient scenarios.

Two distinct methods of solution are demonstrated for the solution of these time-dependent equations. The first approach uses Laplace transforms. The two-group analytical steady state solution is modified to be the image function and inverted using a numerical Laplace transform inversion (NLTI) developed in [3]. The second approach is a more conventional one using the point kinetics equations as derived from the assumption of time/space flux separability. The spatial component comes from the corresponding steady state solution to the basic equations and the temporal factor from the point kinetics model. The novelty here lies in the fact that the elements are generated by the Mathematica computer algebra program to provide essentially exact results. The two solutions will be compared with a third evaluation from a fully numerical code [4]. In this calculation, the spatial variable is discretized by means of a standard finite difference scheme and the time-integration is carried out using a fully implicit Euler scheme.

3. SOLUTION TO THE STEADY STATE EQUATIONS

The appropriate steady state two-group diffusion equations in slab j of n slabs are

$$D_{1j}\frac{d^2\phi_{1j}}{dx^2} - \Sigma_{r1j}\phi_{1j}(x) + \nu\Sigma_{f2j}\phi_{2j}(x) + \nu\Sigma_{f1j}\phi_{1j}(x) = -Q_{1j}(x), \tag{1a}$$

$$D_{2j}\frac{d^2\phi_{2j}}{dx^2} - \Sigma_{r2j}\phi_{2j}(x) + \nu\Sigma_{12j}\phi_{1j}(x) = -Q_{2j}(x), \tag{1b}$$

where the possibility of a nonuniform source $Q_{gj}(x)$ in each region j and group g has been included. It is still assumed that the reactor is symmetric about the centerline and that the exposed surface does not support a flux giving the following external boundary conditions for each group:

$$\left.\frac{d\phi_{g1}}{dx}\right|_0 = 0, \qquad \phi_{gn}(x_n) = 0\ . \tag{1c}$$

As indicated in Fig.1, the surfaces between the homogeneous regions are numbered from the left beginning at 0. Continuity of the flux and current for each group at the interfacial boundaries therefore requires

$$\begin{aligned} \phi_{g,j-1}(x_{j-1}) &= \phi_{g,j}(x_{j-1}), \\ -D_{g,j-1}\left.\frac{\partial\phi_{g,j-1}(x)}{\partial x}\right|_{x=x_{j-1}} &= -D_{g,j}\left.\frac{\partial\phi_{g,j}(x)}{\partial x}\right|_{x=x_{j-1}}. \end{aligned} \tag{1d}$$

A more convenient form for Eqs. (1a) and (1b) is

$$\begin{bmatrix} \frac{d^2}{dx^2}+\gamma_{11} & \gamma_{12} \\ \gamma_{21} & \frac{d^2}{dx^2}-\gamma_{22} \end{bmatrix} \vec{\Phi}_j(x) = -\begin{bmatrix} \frac{Q_{1j}}{D_{1j}} \\ \frac{Q_{2j}}{D_{2j}} \end{bmatrix} \tag{2a}$$

where the γ-matrix and the group vector for each region j are defined as

$$\begin{aligned} \gamma_{11} &\equiv \frac{\nu\Sigma_{f1j}-\Sigma_{r1j}}{D_{1j}}, & \gamma_{12} &\equiv \frac{\nu\Sigma_{f2j}}{D_{2j}}, \\ \gamma_{21} &\equiv \frac{\Sigma_{12j}}{D_{2j}}, & \gamma_{22} &\equiv \frac{\Sigma_{r2j}}{D_{2j}}, \end{aligned} \tag{2b}$$

$$\vec{\Phi}_j(x) = \begin{bmatrix} \phi_{1j}(x) & \phi_{2j}(x) \end{bmatrix}^T, \tag{2c}$$

where T denotes the vector transpose. The particular solution vector $\vec{q}_j$ for uniform regional sources can be obtained from the solution of

$$\underline{\gamma}_j \vec{q}_j = -\underline{D}_j^{-1}\vec{Q}_j, \tag{3a}$$

where

$$\underline{D}_j^{-1} \equiv \begin{bmatrix} 1/D_{j1} & 0 \\ 0 & 1/D_{j2} \end{bmatrix}, \qquad \vec{Q}_j \equiv \begin{bmatrix} Q_{1j} \\ Q_{2j} \end{bmatrix},$$

giving

$$\vec{q}_j = \begin{bmatrix} -\dfrac{\gamma_{22}\dfrac{Q_{1j}}{D_{1j}} + \gamma_{12}\dfrac{Q_{2j}}{D_{2j}}}{\gamma_{11}\gamma_{22} + \gamma_{12}\gamma_{21}} \\ \dfrac{\gamma_{11}\dfrac{Q_{2j}}{D_{2j}} - \gamma_{21}\dfrac{Q_{1j}}{D_{1j}}}{\gamma_{11}\gamma_{22} + \gamma_{12}\gamma_{21}} \end{bmatrix}. \tag{3b}$$

As suggested from the one-group formulation [3], we seek a solution in each region as a sum homogeneous and particular solutions

$$\vec{\Phi}_j(x) = \underline{A}_j(x)\left(\vec{\Phi}_j - \vec{\Phi}_{pj}^{+}\right) + \hat{\underline{B}}_j(x)\left(\vec{\Phi}_{j-1} - \vec{\Phi}_{pj}^{-}\right) + \vec{\Phi}_{pj}(x), \tag{4a}$$

where

$$\begin{aligned} &\vec{\Phi}_j \equiv \vec{\Phi}_j\left(x_j\right), \qquad &&\vec{\Phi}_{j-1} \equiv \vec{\Phi}_{j-1}\left(x_{j-1}\right), \\ &\vec{\Phi}_{pj}^{+} \equiv \vec{\Phi}_{pj}\left(x_j\right), \qquad &&\vec{\Phi}_{pj}^{-} \equiv \vec{\Phi}_{pj}\left(x_{j-1}\right). \end{aligned} \tag{4b}$$

From Eq. (3b), we have that the particular solution is

$$\vec{\Phi}_{pj}^{\pm} = \vec{q}_j .$$

To be a proper solution giving the appropriate boundary fluxes, the matrices $\underline{A}_j(x)$ and $\hat{\underline{B}}_j(x)$ must satisfy

$$\begin{aligned} &\underline{A}_j\left(x_j\right) = \underline{I}, \quad \underline{A}_j\left(x_{j-1}\right) = \underline{0}, \\ &\hat{\underline{B}}_j\left(x_j\right) = \underline{0}, \quad \hat{\underline{B}}_j\left(x_{j-1}\right) = \underline{I}. \end{aligned} \tag{5}$$

The interfacial coefficient vector $\vec{\Phi}_j$ is not yet specified but will momentarily be determined from current continuity.

Each homogeneous component of the solution

$$\vec{\Psi}(x) = \underline{A}_j(x)\vec{a} + \hat{\underline{B}}_j(x)\vec{b}, \tag{6a}$$

is assumed to satisfy

$$\underline{\nabla}^2\vec{\Psi}^i(x) + B^2\vec{\Psi}^i(x) = \vec{0}, \tag{6b}$$

where the matrix operator is

$$\underline{\nabla}^2 \equiv \quad diag\left[\frac{d^2}{dx^2}, \quad \frac{d^2}{dx^2}\right].$$

The appropriate eigenvalues B for which Ψ^i is solution can be found by substitution of Eq. (6a) into homogeneous form of Eq. (2a) to give

$$\begin{bmatrix} -B^2+\gamma_{11} & \gamma_{12} \\ \gamma_{21} & -B^2-\gamma_{22} \end{bmatrix} \vec{\Psi}^i(x) = \vec{0}\,. \tag{6c}$$

This equation has a nontrivial solution if and only if the determinant of the coefficient matrix vanishes to yield the region-wise eigenvalues

$$B_{12}^2 \equiv \frac{1}{2}\left[\left(\gamma_{11}-\gamma_{22}\right) \pm \sqrt{\left(\gamma_{11}-\gamma_{22}\right)^2+4\left(\gamma_{11}\gamma_{22}+\gamma_{12}\gamma_{21}\right)}\right]. \tag{6d}$$

When Eq. (6a) is introduced into Eq. (6b) and if $\vec{a}$ and $\vec{b}$ are to be arbitrary, the following fundamental matrix equations result for $\underline{A}_j(x)$ and $\underline{\hat{B}}_j(x)$

$$\underline{\nabla}^2 \underline{A}_j(x) + B^2 \underline{A}_j(x) = \underline{0}\,,$$
$$\underline{\nabla}^2 \underline{\hat{B}}_j(x) + B^2 \underline{\hat{B}}_j(x) = \underline{0}\,.$$

Since there will be 4 eigenvalues, each group will therefore admit 4 homogeneous solutions which when summed can be put into the form

$$\begin{aligned}\Psi_g(x) = C_{g1}\chi\left[B_1\left(x-x_{j-1}\right)\right] + C_{g2}\chi\left[B_1\left(x_j-x\right)\right] + \\ + C_{g3}\chi\left[B_2\left(x-x_{j-1}\right)\right] + C_{g4}\chi\left[B_2(x_j-x)\right],\end{aligned} \tag{7a}$$

where depending upon the sign of B_{12}^2 the appropriate branch of χ is chosen as

$$\chi(\beta x) \equiv \begin{cases} \sinh(\beta x), \beta^2 < 0 \\ \sin(\beta x), \beta^2 > 0\,. \end{cases} \tag{7b}$$

But also each independent homogeneous solution must satisfy the second (or first) equation of Eq. (6c) for each eigenvalue

$$-D_{2j}B_j^2\Psi_{2j}^i(x) - \Sigma_{r2j}\Psi_{2j}^i(x) + \Sigma_{12j}\Psi_{1j}^i(x) = 0 \tag{8a}$$

which gives

$$\Psi_{2j}^{i}(x)=\alpha_j\left(B_j\right)\Psi_{1j}^{i}(x),$$
$$\alpha_j\left(B_j\right)\equiv\frac{\Sigma_{12j}}{\Sigma_{2j}}\frac{1}{1+B_j^2L_{2j}^2}, \tag{8b}$$
$$L_{2j}^2\equiv\frac{D_{2j}}{\Sigma_{r2j}}\ .$$

Thus

$$\begin{aligned}C_{21}&=\alpha_{1j}C_{11},\quad C_{22}=\alpha_{1j}C_{12},\\ C_{23}&=\alpha_{2j}C_{13},\quad C_{24}=\alpha_{2j}C_{14},\end{aligned} \tag{9}$$

where $\alpha_{gj}\equiv\alpha(B_{gj})$. If

$$\chi_{gj}^{+}(x)\equiv\chi\left[B_{gj}\left(x-x_{j-1}\right)\right],\quad \chi_{gj}^{-}(x)\equiv\chi\left[B_{gj}\left(x_j-x\right)\right],$$

for convenience, then the homogeneous solution [Eq. (7a)] can be recast as

$$\begin{aligned}\vec{\Psi}(x)=&\begin{bmatrix}1 & 1\\ \alpha_{1j} & \alpha_{2j}\end{bmatrix}\begin{bmatrix}\chi_{1j}^{+}(x) & 0\\ 0 & \chi_{2j}^{+}(x)\end{bmatrix}\begin{bmatrix}C_{11}\\ C_{13}\end{bmatrix}+\\ &+\begin{bmatrix}1 & 1\\ \alpha_{1j} & \alpha_{2j}\end{bmatrix}\begin{bmatrix}\chi_{1j}^{-}(x) & 0\\ 0 & \chi_{2j}^{-}(x)\end{bmatrix}\begin{bmatrix}C_{12}\\ C_{14}\end{bmatrix}.\end{aligned} \tag{10}$$

If Eq. (10) is evaluated at x_j and x_{j-1} respectively, we have

$$\begin{aligned}\vec{\Psi}_j&=\begin{bmatrix}1 & 1\\ \alpha_{1j} & \alpha_{2j}\end{bmatrix}\begin{bmatrix}\chi_{1j} & 0\\ 0 & \chi_{2j}\end{bmatrix}\begin{bmatrix}C_{11}\\ C_{13}\end{bmatrix},\\ \vec{\Psi}_{j-1}&=\begin{bmatrix}1 & 1\\ \alpha_{1}j & \alpha_{2j}\end{bmatrix}\begin{bmatrix}\chi_{1j} & 0\\ 0 & \chi_{2j}\end{bmatrix}\begin{bmatrix}C_{12}\\ C_{14}\end{bmatrix}\end{aligned} \tag{11}$$

which when solved for $C_{i,j}$ and substituted into Eq. (10) gives

$$\vec{\Psi}_j(x)=\left[\underline{\alpha}_j\underline{h}_j^{+}(x)\underline{\alpha}_j^{-1}\right]\vec{\Psi}_j+\left[\underline{\alpha}_j\underline{h}_j^{-}(x)\underline{\alpha}_j^{-1}\right]\vec{\Psi}_{j-1}, \tag{12}$$

with

$$\underline{\alpha}_j \equiv \begin{bmatrix} 1 & 1 \\ \alpha_{1j} & \alpha_{2j} \end{bmatrix},$$

$$\underline{h}_j^{\pm}(x) \equiv \begin{bmatrix} \chi_{1j}^{\pm}(x)/\chi_{1j} & 0 \\ 0 & \chi_{2j}^{\pm}(x)/\chi_{2j} \end{bmatrix},$$

and

$$\chi_{gj} \equiv \chi\left(B_{gj}\Delta_j\right).$$

Thus, it is evident from Eq. (4a) that

$$\begin{aligned} \underline{A}_j(x) &\equiv \underline{\alpha}_j \underline{h}_j^{+}(x)\underline{\alpha}_j^{-1}, \\ \underline{\hat{B}}_j(x) &\equiv \underline{\alpha}_j \underline{h}_j^{-}(x)\underline{\alpha}_j^{-1}. \end{aligned} \tag{13}$$

As for the one-group case [3], the advantage of this particular form of the solution is realized when the interfacial current conditions are satisfied to give the following 3-point vector recurrence relation for the coupling coefficient vector:

$$\underline{M}_j\vec{\Phi}_j - \underline{N}_j\vec{\Phi}_{j-1} - \underline{P}_j\vec{\Phi}_{j-2} = \vec{f}_j, \qquad 2 \le j \le n \tag{14a}$$

with

$$\underline{M}_j \equiv \underline{D}_j \left.\frac{d\underline{A}_j}{dx}\right|_{x_{j-1}},$$

$$\underline{N}_j \equiv \underline{D}_{j-1} \left.\frac{d\underline{A}_{j-1}}{dx}\right|_{x_{j-1}} - \underline{D}_j \left.\frac{d\underline{B}_j}{dx}\right|_{x_{j-1}},$$

$$\underline{P}_j \equiv \underline{D}_{j-1} \left.\frac{d\underline{B}_j}{dx}\right|_{x_{j-1}},$$

$$\vec{f}_j \equiv \underline{D}_j \left[\left.\frac{d\underline{A}_j}{dx}\right|_{x_{j-1}} + \left.\frac{d\underline{B}_j}{dx}\right|_{x_{j-1}}\right]\vec{\Phi}_{pj} - \underline{D}_{j-1}\left[\left.\frac{d\underline{A}_{j-1}}{dx}\right|_{x_{j-1}} + \left.\frac{d\underline{B}_{j-1}}{dx}\right|_{x_{j-1}}\right]\vec{\Phi}_{pj-1},$$

$$\underline{D}_j \equiv diag\left[D_{1j}, D_{2j}\right].$$

The symmetry condition at the ADS center

$$\left.\frac{d\vec{\Phi}_0}{dx}\right|_{x=0} = 0$$

implies

$$\vec{\Phi}_0 = (\underline{I} + \underline{E})\vec{\Phi}_{p1} - \underline{E}\vec{\Phi}_1, \tag{15}$$

where

$$\underline{E} \equiv \left[\left.\frac{d\underline{B}_1}{dx}\right|_0\right]^{-1} \left.\frac{d\underline{A}_1}{dx}\right|_0,$$

yielding a modified equation for j=2

$$\underline{M}_2\vec{\Phi}_2 - \underline{N}_2\vec{\Phi}_1 = \vec{f}_2{}', \tag{14b}$$

with

$$\underline{N}_2 \equiv \left[\underline{D}_1 \left.\frac{d\underline{A}_1}{dx}\right|_{x_1} - \underline{D}_2 \left.\frac{d\underline{B}_2}{dx}\right|_{x_1}\right] - \underline{D}_1 \left.\frac{d\underline{B}_1}{dx}\right|_{x_1} \underline{E},$$

$$\vec{f}_2{}' = \vec{f}_2 + \underline{D}_1 \left.\frac{d\underline{B}_1}{dx}\right|_{x_1} (\underline{I} + \underline{E})\vec{\Phi}_{p1} .$$

Now, we can specify, without loss of generality, that

$$\vec{\Phi}_0 \equiv \vec{0}.$$

The vector recurrence given by Eqs. (14) is one of the boundary value type, i.e., $\vec{\Phi}_0$ and $\vec{\Phi}_n$ are specified rather than $\vec{\Phi}_0$ and $\vec{\Phi}_1$. The solution can most conveniently be obtained via a block tri-diagonal solver.

In addition, the steady state equations [Eqs. (1)] are solved analytically in each region using for instance Mathematica. In the central layers, fission increases the coupling between the regions in such a way that the "local" bucklings satisfy fourth degree polynomial equations. Analytical manipulation is performed on the neutron fluxes to exhibit the (unknown) values of the fluxes at the layer interfaces. Patching all local solutions together by requiring continuity of the neutron currents at the interfaces, gives a 6x6 (block-diagonal) algebraic system that is relatively easy to invert.

Once the neutron fluxes have been determined, an estimation (usually called "source" multiplication factor k_{source}) of the eigenvalue may be obtained through the ratio

$$k_{source} = \frac{(\vec{w}, J\vec{\Phi})}{(\vec{w}, K\vec{\Phi})} \tag{15}$$

of neutron production and neutron losses. In this expression J and K denote the fission and annihilation (i.e. removal and leakage) operators, $\vec{\Phi}(x)$ refers to the vector of neutron fluxes, $\vec{w}(x)$ to a vector of some weighting functions and $(\vec{u}, \vec{v})$ is a scalar product in the physical domain. Since, in steady state, Eqs. (1) may be cast into $K\vec{\Phi}(x) = J\vec{\Phi}(x) + \vec{Q}(x)$, the source multiplication factor becomes:

$$k_{source} = \frac{(\vec{w}, J\vec{\Phi})}{(\vec{w}, J\vec{\Phi}) + (\vec{w}, \vec{Q})}. \tag{16}$$

The quadrature terms in (15) may be evaluated exactly, giving an (usually close) approximation to k_{eff}.

4. SOLUTION TO THE TIME-DEPENDENT EQUATIONS

When the Laplace transform of the basic time-dependent equations is taken, the following "steady state-like" equation results for the transformed flux:

$$\begin{bmatrix} \frac{d^2}{dx^2} + \gamma_{11}(s) & \gamma_{12}(s) \\ \gamma_{21}(s) & \frac{d^2}{dx^2} - \gamma_{22}(s) \end{bmatrix} \vec{\Phi}_j(x,s) = -\begin{bmatrix} \frac{Q_{1j}(s)}{D_{1j}} \\ \frac{Q_{2j}(s)}{D_{2j}} \end{bmatrix}, \tag{17a}$$

with

$$\begin{aligned} \gamma_{11}(s) &\equiv \frac{(1-\beta)\nu\Sigma_{f1j} - \left(\Sigma_{rj} + {}^{s/v}{}_1\right)}{D_{1j}} + \left[1 - \beta + \frac{\lambda\beta}{s+\lambda}\right]\frac{\nu\Sigma_{f1j}}{D_{1j}}, \\ \gamma_{12}(s) &\equiv \left[1 - \beta + \frac{\lambda\beta}{s+\lambda}\right]\frac{\nu\Sigma_{f2j}}{D_{2j}}, \\ \gamma_{21}(s) &\equiv \frac{\Sigma_{12j}}{D_{2j}}, \\ \gamma_{22}(s) &\equiv \frac{\left(\Sigma_{r2j} + {}^{s/v}{}_2\right)}{D_{2j}}. \end{aligned} \tag{17b}$$

and s is the variable in image space. For this case, zero initial conditions were assumed. Specific initial conditions will be treated in the following section. Thus Eq. (4a) becomes the image function when B^2 (now complex) is determined from Eq. (6c) and the particular solution from Eq. (3b)

$$\vec{\Phi}_j(x,s) = \underline{A}_j(x,s)\left(\vec{\Phi}_j(s) - \vec{\Phi}^+_{pj}(s)\right) + \hat{\underline{B}}_j(x,s)\left(\vec{\Phi}_{j-1}(s) - \vec{\Phi}^-_{pj}(s)\right) + \vec{\Phi}_{pj}(x,s), \qquad (18)$$

with

$$\chi(\beta x) \equiv \sin[\beta(s)x].$$

All symbols remain identical to these of the steady state case above with the exception of the γ-matrix defined by Eq. (17b). Equation (18) then serves as the image function to be introduced into the numerical Laplace transform inversion described in the following section.

So far the ADS system has been assumed to start from a zero flux. More realistic cases of starting from steady state should also be considered. For instance, one may assume that the source level in the spallation region changes according to a prescribed function of time from a steady state condition. The initial condition then is the steady state condition at the original source level. The above analysis remains essentially unchanged if the new group vector

$$\vec{\Theta}_j(x,t) \equiv \vec{\Psi}_j(x) - \vec{\Phi}_j(x,t), \qquad (19)$$

is defined and solved for. $\vec{\Psi}_j$ is the steady state group vector. Thus only the change from steady state is to be determined. The only change in the above kinetic equation is that the spallation source now becomes

$$\Delta\vec{S}_j = \vec{Q}_{j0}(x) - \vec{Q}_j(x,t),$$

where $\vec{Q}_j(x,t)$ is the prescribed source trace and $\vec{Q}_{j0}(x)$ is the original source level. Several source trace scenarios will be considered in the results section.

A change in capture cross sections in either (or both) groups in a region, from steady state operation, should also be considered. Again the above formulation is unchanged for the change from steady state, if the transform of the particular solution is

$$\vec{\Theta}_{pj}(x,s) \equiv \frac{1}{s}\left[\underline{C}_j(s)\vec{\Psi}_j(x) + \vec{d}_j(s)\right], \qquad (20)$$

where

$$\underline{C}_j(s)\underline{\gamma}_j(s) - \underline{\gamma}'_j(s)\underline{C}_j(s) = \begin{bmatrix} \Delta\Sigma_{r1} & 0 \\ 0 & \Delta\Sigma_{r2} \end{bmatrix}$$

and

$$\vec{d}_j = \left[\underline{\gamma}'^{-1}_j C_j(s)\underline{D}^{-1}_j\right]\vec{Q}_j \ .$$

$\underline{\gamma}'_j$ is the γ-matrix with the changed cross sections and $\Delta\Sigma_{rg}$ is the cross section change in group g.

4.1. THE NUMERICAL LAPLACE TRANSFORM INVERSION

The numerical algorithm recently developed takes advantage of the following cosine integral form of the Laplace transform:

$$f(t) = \frac{2e^{\gamma t}}{\pi t} \int_0^{\infty} d\omega \, \mathrm{Re}\, \overline{f}\left(\gamma + i\frac{\omega}{t}\right) \cos(\omega). \tag{21}$$

As suggested by many previous inversion algorithms, the approach of decomposing the cosine integral into integrals over the cosine periods will be followed to give

$$f(t) = \frac{2e^{\gamma t}}{\pi t} \sum_{k=0}^{\infty} (-1)^k \int_0^{\pi} d\omega \, \mathrm{Re}\, \overline{f}\left(\gamma + i\frac{\omega + k\pi}{t}\right) \cos(\omega). \tag{22}$$

Each termwise integration is performed using the Romberg integration rule [5] featuring the re-use of function values. If

$$g(\omega) \equiv \mathrm{Re}\, \overline{f}\left(\gamma + i\frac{\omega + k\pi}{t}\right),$$

the Romberg rule is

$$T_l^{m+1} = T_l^m + \frac{T_l^m - T_{l-1}^m}{4^{m+1} - 1}, \tag{23a}$$

initiated by the trapezoidal rule

$$T_l^0 = \frac{1}{2} T_{l-1}^0 + \frac{\pi}{2^l} \sum_{j=1,odd}^{2^l - 1} g\left(\frac{j\pi}{2^l}\right), \quad T_0^0 = \frac{\pi}{2}[g(0) + g(\pi)] \ . \tag{23b}$$

The central feature of the algorithm is acceleration to convergence of the series in Eq. (21) using the nonlinear Wynn-epsilon acceleration [6]. The proposed algorithm is made possible only through the efficiency of convergence provided by the epsilon convergence accelerator.

4.2. ERROR CONTROL

As with any numerical algorithm, its truth lies in the details of implementation. Three potential sources of error have been identified in the NLTI algorithm including: (i) numerical quadrature error, (ii) series truncation error, and (iii) loss of significance.

With regard to numerical quadrature errors, the diagonal elements of the tableau formed by the approximations T_l^m are monitored for convergence using the relative error between two successive Romberg approximations

$$\varepsilon_{R1} \equiv \left| \frac{T_l^{m+1} - T_l^m}{T_l^{m+1}} \right| . \tag{24}$$

In addition, the relative error between trapezoidal quadratures is also monitored

$$\varepsilon_{R2} \equiv \left| \frac{T_{l+1}^0 - T_l^0}{T_{l+1}^{m+1}} \right|, \tag{25}$$

for convergence. The integration is considered converged when $\min(\varepsilon_{R1}, \varepsilon_{R2}) \le \varepsilon$ where ε is the desired relative error for the inversion under consideration. In parallel, the trapezoidal integration and the diagonal elements are considered sequences in *l* and *m* respectively. The epsilon algorithm is applied to each sequence to accelerate convergence and ε_{R2} and ε_{R1} are replaced by the errors associated with the acceleration if smaller.

The Wynn-epsilon algorithm for the convergence of a sequence tending to a limit can be written as

$$\begin{aligned} &\varepsilon_{-1}^{(n)} = 0,\ \varepsilon_0^{(n)} = S_n, \\ &\varepsilon_{k+1}^{(n)} = \varepsilon_k^{(n+1)} + \left[\varepsilon_k^{(n+1)} - \varepsilon_k^{(n)} \right]^{-1}, \end{aligned} \tag{26}$$

where S_n is the sequence to be accelerated toward convergence. A tableau is constructed with sequential diagonal elements interrogated for convergence. It could happen that the denominator of the second term in Eq. (26) vanishes leading to erroneous results. This situation is flagged and reported and since exact convergence has apparently been achieved when this happens, $\varepsilon_k^{(n)}$ is assumed to be the converged result. In the normal mode of operation, the final diagonal element of the tableau is returned as the limit to the sequence.

The series truncation error in evaluation Eq. (22) is estimated by

$$\varepsilon_S \equiv \left| \frac{S_n - S_{n-1}}{S_n} \right|, \tag{27}$$

where S_n is either the accelerated epsilon algorithm result or the original partial sum after *n* terms. The epsilon algorithm tableau is created using all partial sums less than or equal to *n*. The series is considered converged when $\varepsilon_s \le \varepsilon$ for two consecutive partial sums.

The final error occurs when summing a series of numbers since there is always the potential for contamination by roundoff due to subtraction. In an attempt to minimize this, the series in Eq. (22) is summed using compensated summation. When the sum is predicted to have converged after *n* terms and if the condition number

$$r \equiv \sum_{k=1}^{n} \left| a_k \right| \Big/ \left| \sum_{k=1}^{n} a_k \right|$$

is larger than $1/\varepsilon$, then potential roundoff error has occurred. In this case, the relative integration error is reduced by a factor of 10 and the summation recalculated until either no roundoff error is predicted or the integration tolerance is below a preset limit. If the sum cannot be computed without roundoff occurring, an error diagnostic is issued.

4.3. POSITIONING OF THE BROMWICH CONTOUR

Not unlike essentially all existing numerical Laplace transform algorithms, there is at least one parameter that needs to be predetermined in order for the algorithm to operate properly. For the present algorithm, the position γ of the Bromwich contour on the real line is critical. While, in theory, γ need only be larger than the real part of the largest singularity, in practice, the numerical evaluation can be extremely sensitive to γ. For this reason, special attention must be given to the choice of γ to ensure reliable results.

Based on [7], an optimization approach will be followed. The optimization, however, will not be for the minimization of an error estimate since an explicit error estimate for the NLTI algorithm is difficult to obtain because of the inclusion of the epsilon algorithm. Instead, an optimization will be based on the minimization of the number of function evaluations. Using the **BRENT** minimization routine [5] and assuming an initial γ and a computational error of a factor of 10 times the desired error ε, γ is determined to give a local minimum number of function evaluations for a given *t*. This is done in order to minimize computation time. While the minimum found might not be a global one, it is hoped that the γ found will allow the inversion to proceed. However, at this point in the evaluation, there is no guarantee that the inversion obtained is indeed accurate. To provide a sense of accuracy, the error is decreased by a factor of 10 (to ε) and the inversion recalculated. This procedure is continued until either the relative error between two successive approximations is less than the desired error or ε has been reduced twice at which time a "failed error check" is indicated. The implementation of this error check is accomplished by reusing all previous function evaluations for each subsequent determination. In this way, the total computation time is reduced.

5. NUMERICAL RESULTS

The above algorithm for the steady state ADS has been implemented (in a slightly different version) using both Mathematica and a Fortran program. The latter was run on a SUN Ultra 5 workstation. The nominal ADS nuclear parameters found in Table 1

were used to all digits presented. The two-group analytical neutron fluxes given by Mathematica are the following (all digits are exact) :

1/. Spallation source region

$$\phi_1(x) = 37.8996795110680 + 59.337170293103\cosh(0.07696020516499192\,x), \quad (28)$$

$$\phi_2(x) = 197.0157829229451 + 299.546799513879\cosh(0.04588380532185835\,x) - 105.1958215570534\cosh(0.07696020516499192\,x), \quad (29)$$

2/. Fuel region 1

$$\phi_1(x) = 101.2326237183662\cos(0.05645646205748660\,x) - 34.3408565002764\cosh(0.1522503619720471\,x) + 67.2389213998901\sin(0.05645646205748660\,x) + 33.5234933528605\sinh(0.1522503619720471\,x), \quad (30)$$

$$\phi_2(x) = 303.208290266751\cos(0.05645646205748660\,x) + 90.320728470628\cosh(0.1522503619720471\,x) + 201.391583544845\sin(0.05645646205748660\,x) - 88.170961620781\sinh(0.1522503619720471\,x), \quad (31)$$

3/. Fuel region 2

$$\phi_1(x) = 109.2793541507429\cos(0.04595652099141732\,x) + 33.604197709720\cosh(0.1501776444464567\,x) + 37.4447366476900\sin(0.04595652099141732\,x) - 33.825257619323\sinh(0.1501776444464567\,x), \quad (32)$$

$$\phi_2(x) = 381.795074948647\cos(0.04595652099141732\,x) - 91.90011369826\cosh(0.1501776444464567\,x) + 130.822662212265\sin(0.04595652099141732\,x) + 92.50466408813\sinh(0.1501776444464567\,x), \quad (33)$$

4/. Reflector

$$\phi_1(x) = 0.3037223763443253\sinh(8.14721719559198 - 0.0775925447199236\,x), \quad (34)$$

$$\phi_2(x) = -0.617689205588614\sinh(8.14721719559198 - 0.0775925447199237\,x) + 20.54220270049755\sinh(4.90038073339705 - 0.04667029269901952\,x). \quad (35)$$

A k_{source} of 0.9479824648 was then obtained from Eq. (16) in close agreement with the multiplication factor obtained from the singularity of the system requiring the reactor to sustain neutron fluxes in the absence of external sources: k_{eff} = 0.9500206. The flux distribution (28)-(35) and eq(4a) was compared to a finite difference calculations and the results are shown on Fig. 2. From this comparison, we can safely conclude that the ADS steady state two-group calculation either coded in FORTRAN or by Mathematica are operational and ready to serve as the basis for the transient case.

5.1. TRANSIENT APPROACH TO STEADY STATE

Figure 3a shows the transient approach of the flux to its critical distribution. For this case, the initial flux was assumed to be zero and the source was assumed to be pulsed at time zero giving the source transform independent of *s*. The fission cross sections were divided by k_{eff} to give a critical system. This is a particularly stringent test in

that small deviations from the true k_{eff} would promote instability at long times. Here we see that the reactor achieves criticality at 10^{-2} s which is maintained to at least 10^{2} s. At longer times, the inversion seems to break down which is probably a matter of adjusting the Bromwich contour. This issue is currently being addressed.

Figure 3b shows the transient at the material interfaces for the steady state of Fig. 2. For this case, the source is turned on with zero flux at $t = 0$. Steady state is achieved at about 10 s after an apparent steady state owing to the effect of delayed neutrons. This calculation is stable to 10^{4} s and longer. The success of this calculation indicates that the inversion is indeed working properly and can be robust for certain scenarios. The fully numerical calculation produces results which are in excellent agreement with the reference.

5.2 EXPONENTIAL SOURCE TRACE TO A NEW STEADY STATE

For this case, the source level was increased by a factor 2 to generate a new steady state condition. The source trace was such that the approach from the original to new source was exponential (with exponent α=10)

$$\Delta\vec{S}(x,t) = \vec{Q}_0 + \left(1 - e^{-\alpha t}\right)\Delta\vec{Q},$$

giving the source transform

$$\Delta\vec{Q}(x,s) = -\frac{\alpha}{s(s+\alpha)}(f_S - 1)\vec{Q}_{j0}.$$

Figure 4 shows the resulting group flux differences from the original steady state for a source reduction of a factor of 2. Initially nothing happens as the source slowly increases. Then the new source begins to dominate and a new steady state is reached. Note that the difference is negative indicating an increase to the initial steady state flux [see eq(19)]

5.3 POINT KINETICS

Finally, point kinetics was used to analyze a transient where the group-2 capture cross section Σ_{r2} in fuel region 1 was instantaneously lowered by 10% (i.e. from 8.43028 (-3) cm^{-1} to 7.58725 (-3) cm^{-1}). The reactor core remains subcritical as shown by a numerical evaluation of the new k_{eff}. This cross section modification initiates a power transient that starts from the initial steady state with *T(0)=1*, where *T(t)* is the amplitude in the classical separation solution technique (i.e. $\vec{\Phi}(x,t) = \vec{\Psi}(x)\,T(t)$ with $\vec{\Psi}(x)$ the steady state flux distribution). The point kinetics equations were solved analytically using Mathematica yielding an asymptotic amplitude equal to $T(\infty)$ = 2.1248230520055807 (all digits exact). Figure 5 shows the steady state flux distribution corresponding to the new cross section set, compared to the asymptotic point kinetics solution to the transient.

6. CONCLUSIONS

In the present paper a reliable benchmark for accelerator-driven systems has been established in steady-state and transient situations. Benchmark reference results, though limited to highly simplified configurations, are very important in order to get full and detailed physical insight into the phenomena involved and to establish the limits of applicability of models and algorithms which need to be applied when studying realistic situations.
The benchmark has been applied to a system having physical parameters typical of the MYRRHA system which is proposed by the Belgian Nuclear Center of Mol. The results have been compared to fully numerical calculations using standard discretization schemes and to point kinetics. Future work will include more extensive comparisons with numerical techniques usually employed in full-system evaluations, such as quasi-statics and multipoint methods.

REFERENCES

[1] C. Rubbia *et al.*, "A European Roadmap for Developing Accelerator Driven Systems (ADS) for Nuclear Waste Incineration", ENEA Report, May 2001.
[2] C. Rubbia *et al.,* "Conceptual Design of a Fast Neutron Operated High Power Energy Amplifier", Report CERN/AT/ 95-44, 1995.
[3] B.D. Ganapol, R. Furfaro, "Neutron Kinetics via Numerical Laplace Transform Inversion", *Trans Am. Nucl. Soc*., American Nuclear Society Winter Meeting, Washington DC, November 2000.
[4] P. Ravetto, M.M. Rostagno, G. Bianchini, M. Carta, A. D'Angelo, "Application of the Multipoint Method to the Kinetics of Accelerator-Driven Systems", This Conference, 2002.
[5] Press, S.A., Flannery, W.H.., Vettering, W.T., Teukolsky, B.P., *Numerical Recipes*, Cambridge University Press, 1992.
[6] Baker, G.A. and Graves-Morris, P. R, *Padé Approximants*, Cambridge University Press, 1996.
[7] J.A.C. Weideman, *SIAM J. Sci. Comput*., **21**, 111-128, 1999.

Table 1 Dimensions and nuclear properties by group of each region

j	g	$D(cm)$	$\nu\Sigma_f(cm^{-1})$	$\Sigma_r(cm^{-1})$	$\Sigma_{12}(cm^{-1})$	$Q(n/s\text{-}cm^3)$	$\Delta(cm)$
1	1	3.1714	0.00	1.87838e-02	0.0	7.119e-01	6.405
	2	1.8202	0.00	3.83211e-03	1.23190e-02	2.881e-01	
2	1	2.2438	2.19610e-02	4.63106e-02	0.0	0.0	10.542
	2	9.2226e-01	1.05174e-02	8.43028e-03	3.40545e-02	0.0	
3	1	2.2455	1.97980e-02	4.61230e-02	0.0	0.0	10.974
	2	9.1194e-01	8.89230e-03	7.95018e-03	3.45050e-02	0.0	
4	1	2.6501	0.00	1.59552e-02	0.0	0.0	77.079
	2	1.3526	0.00	2.94612e-03	1.05700e-02	0.0	

Table 2 Kinetics Parameters

g	1	2
$\nu(cm/s)$	1.8751e09	3.3188e08

β	0.01446
$\lambda\ (s^{-1})$	0.4265

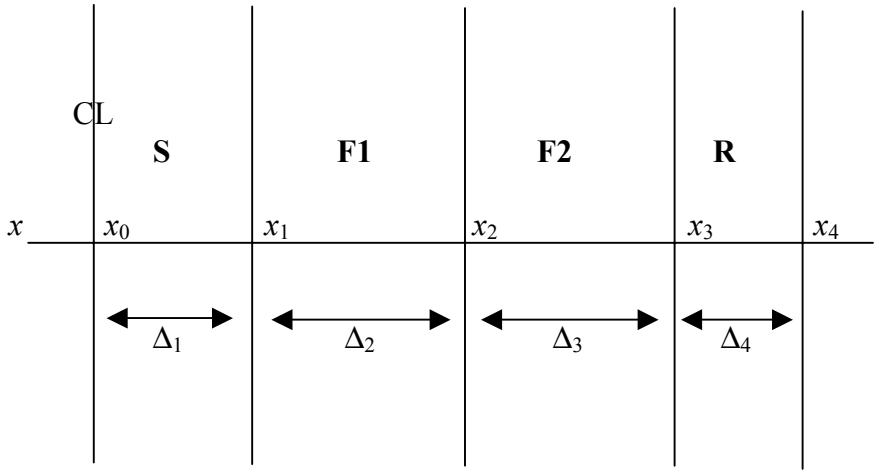

Figure 1. ADS Myrrha concept consist of the following four regions:

S Spallation Source
F1 First Fissile Layer
F2 Second Fissile Layer
R Reflector

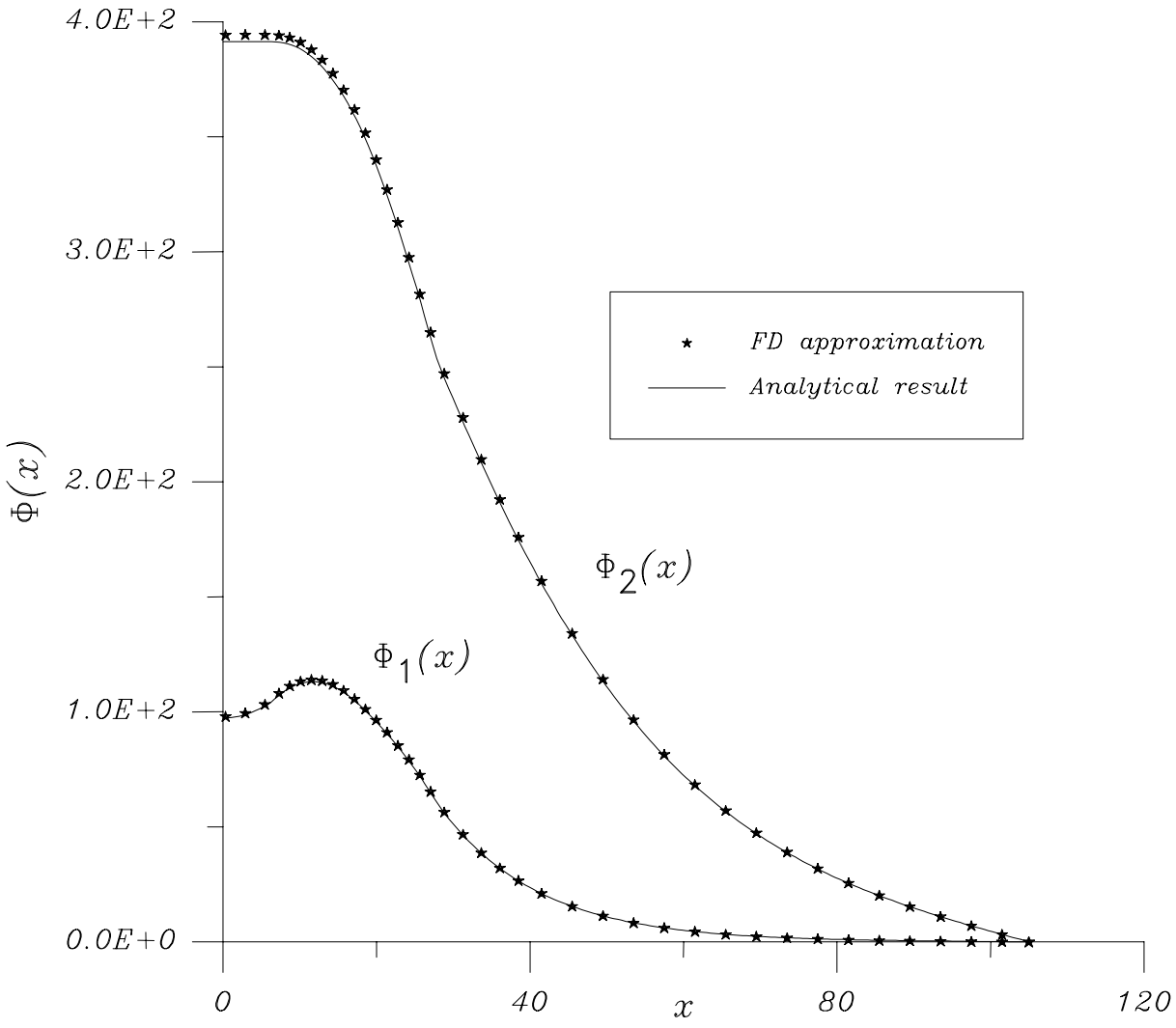

Figure 2. Steady state ADS flux distribution corresponding to the cross section data set and source condition in Table 1.

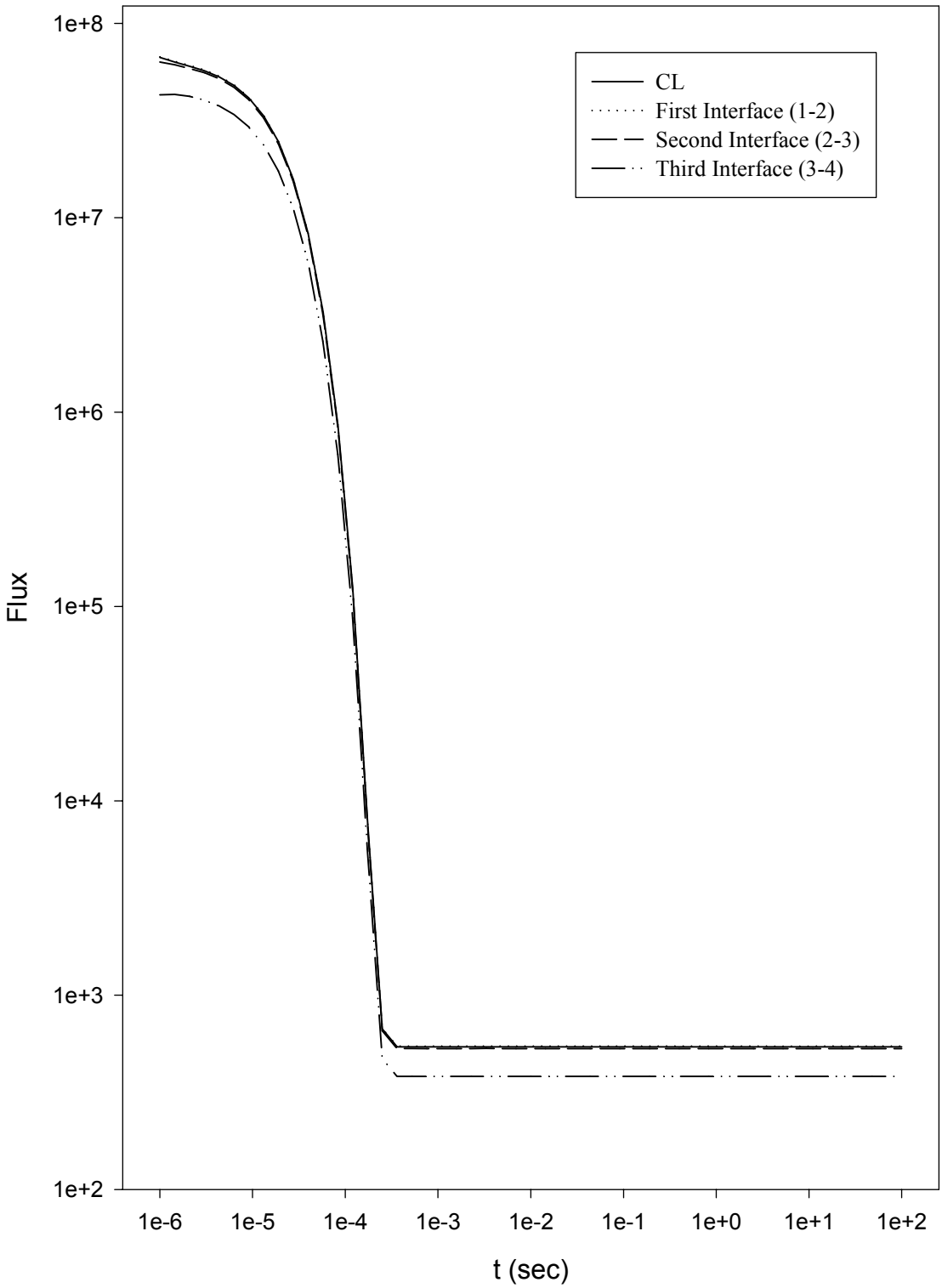

Figure 3a. Approach to critical (k_{eff} = 0.9500206)

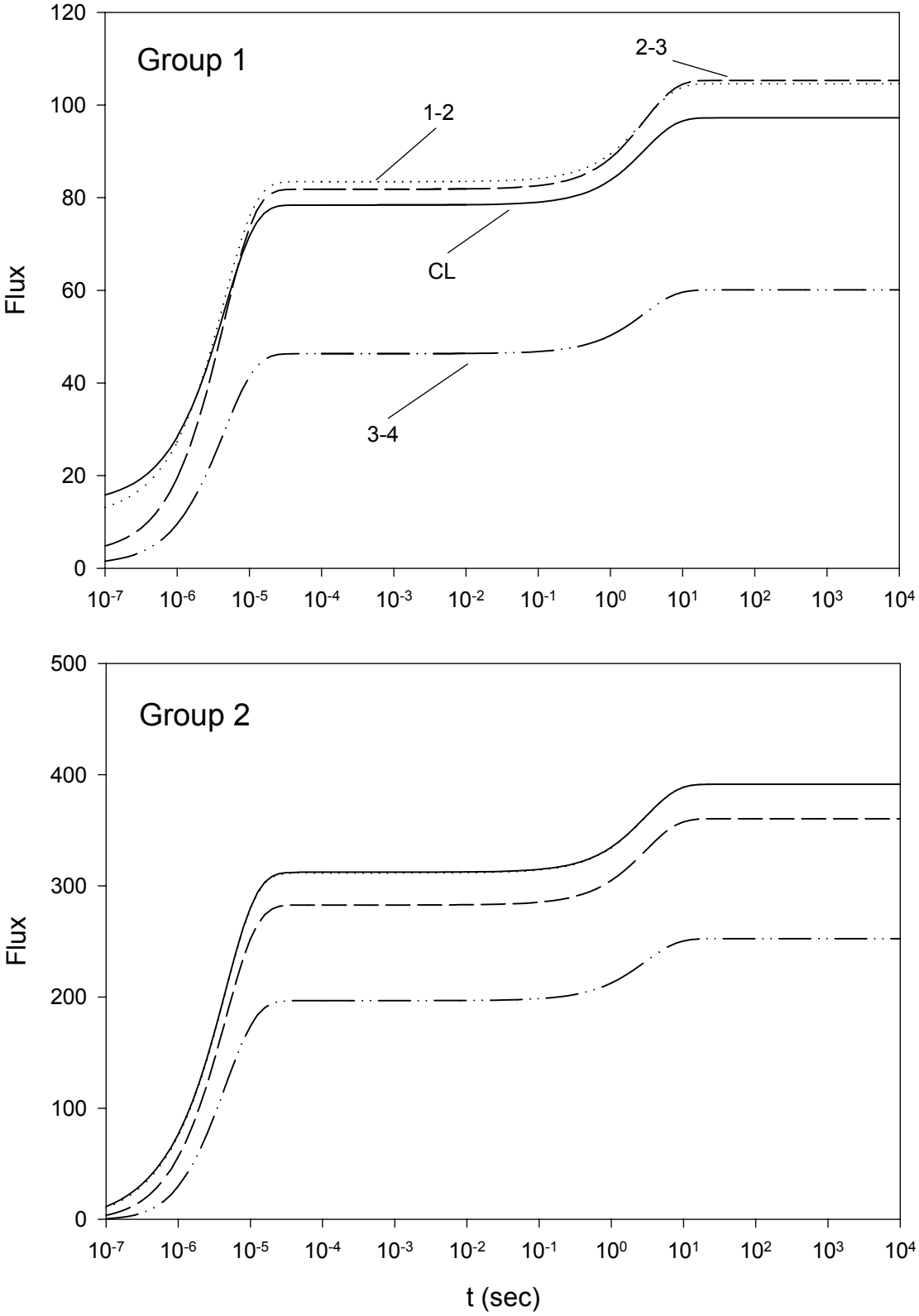

Figure 3b. Approach to steady state at interfaces

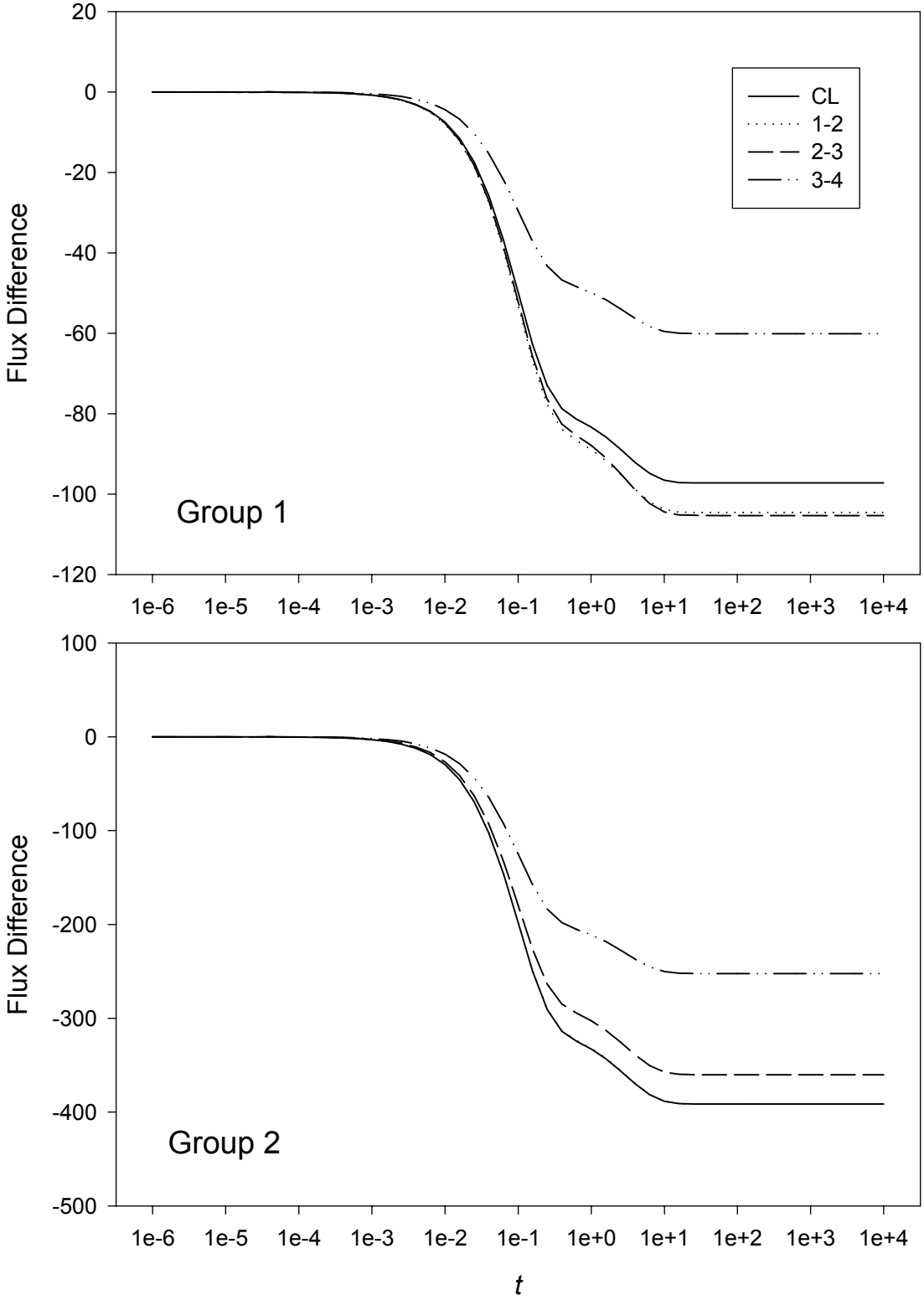

Figure 4. Flux increase by a factor of 2

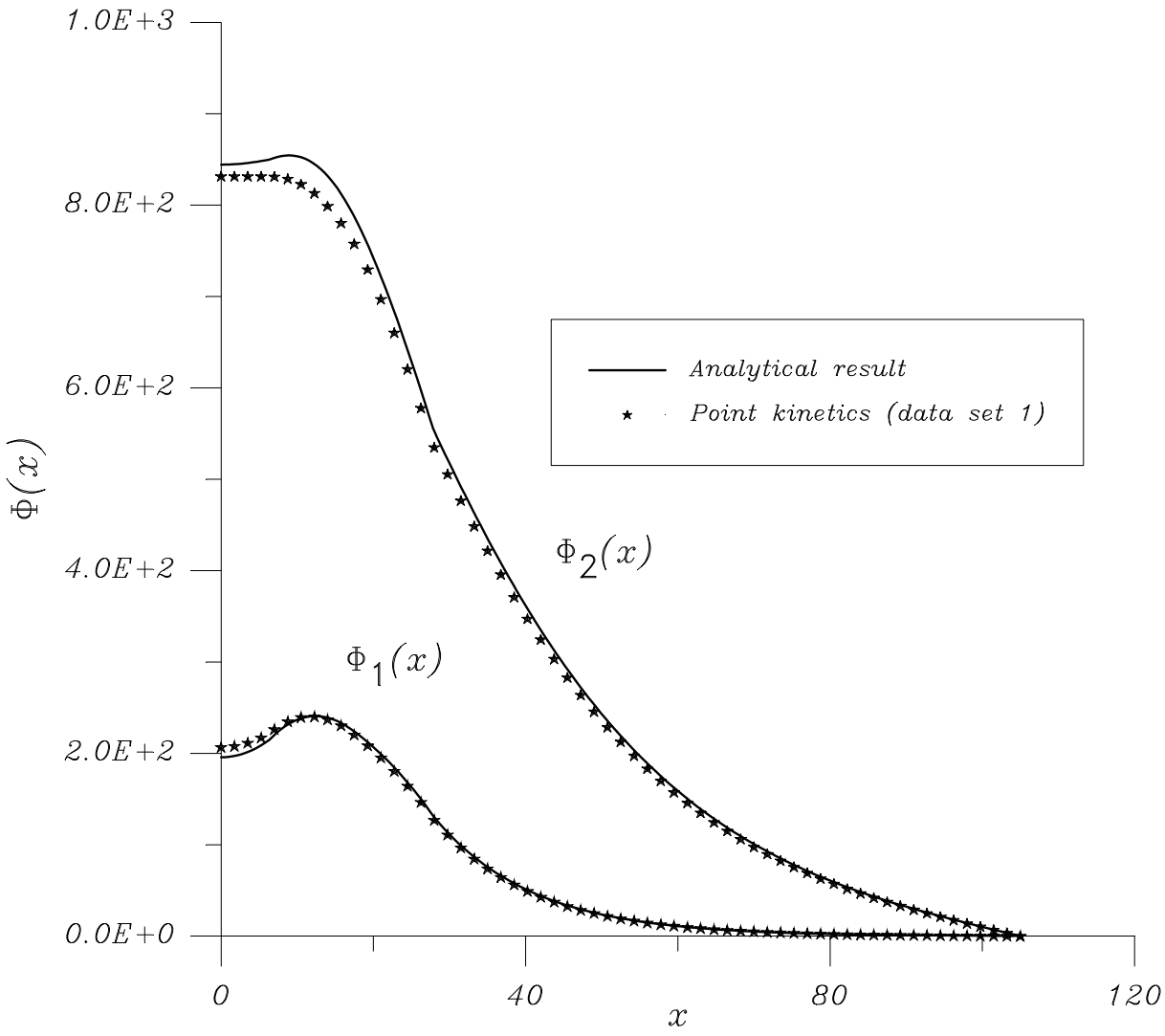

Figure 5. Steady state ADS flux distribution corresponding to the Table 1 cross section data set with a 10% reduction of Σ_{r2} in fuel region 1. This distribution is compared to the point kinetics asymptotic solution to the transient starting from the unperturbed cross section data.